Research Article | Vol. 28, No. 23 / 9 November 2020 / Optics Express 33841

Optics EXPRESS

Two semicircular-hole fiber in a Sagnac loop for simultaneous discrimination of torsion, strain and temperature

LIN HTEIN,[1,4] DINUSHA SERANDI GUNAWARDENA,[1,5] ZHENGYONG LIU,[1,2] AND HWA-YAW TAM[1,3]

[1] *Photonics Research Centre, Department of Electrical Engineering, The Hong Kong Polytechnic University, Kowloon, Hong Kong SAR, China*
[2] *State Key Laboratory of Optoelectronic Materials and Technologies, School of Electronics and Information Technology, Sun Yat-sen University, Guangzhou 510275, China*
[3] *Photonics Research Centre, The Hong Kong Polytechnic University, Shenzhen Research Institute, Shenzhen, China*
[4] *htein.lin@polyu.edu.hk*
[5] *dinusha.gunawardena@polyu.edu.hk*

Abstract: We report a highly sensitive twist sensor based on a Sagnac interferometer constructed with a new type of optical fiber which contains an elliptical core and two large semicircular-holes, where the slow axis of the core orthogonal to the air-holes has a large sensitivity towards twist-induced birefringent changes. The novel fiber structure results in a highest twist sensitivity of 5.01 nm/° at a chosen dip over the range from 370°-400°. The resonance dips in the interference pattern respond with different rates in the wavelength shifts in the presence of physical parameters permitting to experimentally distinguish directional torsion, axial strain and temperature.

1. Introduction

Torsion information is essential for rotating systems, motion tracking in robotic tools and structural health monitoring of large civil structures such as bridges and buildings [1,2]. Torque sensors/transducers which use strain-gauges or magneto elastic materials and angular position sensors can determine twist angles with high accuracy. They are often used in rotating shafts or axles and in in-vehicle applications. Since these types of sensors are generally bulky devices with large dimensions, embedding them in test structures can be rather challenging. In addition, inability to operate in electromagnetic environments and high maintenance limit their applications as well. Optical fibers are immune to electromagnetic interference, and their small size and lightweight offer the possibility to embed them in a variety of structures. A number of optical fiber based twist sensors have been demonstrated including the use of fiber Bragg gratings (FBGs) [3,4], long period gratings (LPGs) [5,6] and interferometers [7,8]. Generally, an optical fiber-based twist sensor suffers from cross-sensitivities of the axial strain and temperature and lacks the capability to distinguish the direction of the twist which is not ideal for practical usage. Several schemes have been proposed to overcome these drawbacks [5,9]. For example, the sensor based on a spirally etched LPG can eliminate the temperature perturbation and distinguish the direction of the applied torsion, but the fabrication process is overly complex.

Twisting of circularly asymmetric fiber can induce mechanical stress around the core and affects the polarization state transformation which results in a change in the interference pattern [10]. In general, a twist sensor based on an optical fiber with asymmetrical air-hole structures in the cladding is more sensitive to twist effect compared to the traditional solid fiber. Therefore, twist sensors based on Sagnac interferometers (SI) have been reported using microstructured optical fibers such as suspended-core fibers [11,12], birefringent photonic crystal fibers (PCFs)

#402925 https://doi.org/10.1364/OE.402925
Journal © 2020 Received 13 Aug 2020; revised 16 Oct 2020; accepted 16 Oct 2020; published 26 Oct 2020

Optics EXPRESS

[13,14], side-leakage PCF [15] and so on. It has been suggested that stress-induced birefringence is severe in optical fibers with large air-filling ratios. A pair of large air-hole structures has been introduced in the cladding of polarization maintaining (PM) side-hole fibers [16,17] to geometrically break the circular symmetry of the fiber. Torsion-induced stress around the fiber core causes an excessive ellipticity of the core that results in an increase of the group birefringence with the increase in twist. Consequently, a different wavelength response is obtained for each dip in the interference pattern while twisting. This effect can be used either to distinguish strain and temperature perturbations from twist sensing or to measure torsion, strain and temperature simultaneously. The twist sensitivity of a fiber with air-hole structures mainly depends on the arrangement of air-holes and the fiber core.

In this study, a two semicircular-hole fiber (TSHF) with a germanium (Ge)-doped elliptical core in the center and two large semicircular-holes in the cladding was incorporated in a Sagnac loop. In contrast to other PCFs and side-hole fibers [13,16,18], as the slow axis of the fiber core is orthogonal to the two semicircular-holes, the separation of adjacent dips in the interference pattern increases with respect to the angle of twist. The sensor is highly sensitive to torsion when pre-twisting the fiber with a length of 16 cm by 370°. The sensor exhibits stable and highly sensitive twist sensing and also has the ability to discriminate the torsion direction. An approach to discriminate torsion, temperature and strain effect is presented by utilizing the different wavelength responses of resonance dips in the interference pattern under applied physical parameters.

2. Fabrication and analysis

The TSHF used as a twist sensor, was fabricated in our laboratory using the stack-and-draw technique. A silica tube with inner and outer diameters of 19 and 25 mm, respectively, was used to hold the structure. A Ge-doped core rod was stacked between two silica slabs which were arranged in a straight line, forming a semicircular-shaped air-hole on each side. The Ge-doped core rod had an elliptical core with dimensions of 0.3×0.7 mm and an outer diameter of ~ 2.5 mm. The two silica slabs had a rectangular shape with dimensions of 2.5×8 mm. The preform was heated up to 1910 °C and drawn to TSHF with a cladding diameter of ~125 µm. The fiber was coated using polyimide with a thickness of 6 µm. The thickness of the strut is ~15 µm and the dimensions of the elliptical core and the air-holes are 2.2×5.3 µm and 38×82 µm, respectively. As shown in the cross-section of the fiber in Fig. 1(a), the slow axis of the elliptical core is orthogonal to the short axes of the air-holes, resulting in a significant difference in the stress distribution along the two polarization axes.

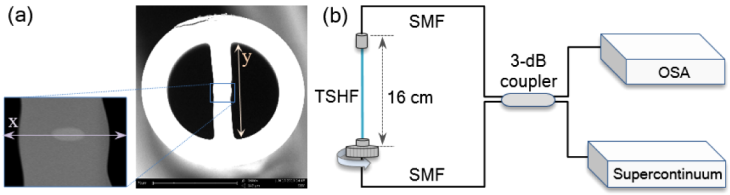

Fig. 1. (a) The SEM image of the TSHF where x and y represent the slow axis of the elliptical core and the long axis of the air-hole, respectively, and (b) experimental setup of the SI-based twist sensor.

The schematic diagram of the twist sensor based on SI is illustrated in Fig. 1(b). The TSHF with a length of 16 cm, which was chosen to optimize the performance of the sensor, was incorporated in a Sagnac loop formed using a 3-dB coupler. Prior to the experiment, the fiber was spliced to a single-mode fiber (SMF) pigtail to measure the splicing loss and attenuation of the TSHF. In the splicing process, the cleaved end of TSHF was positioned ~60 µm away

Optics EXPRESS

from the center of the electrodes of the fusion splicer (FITEL-S178) to avoid collapse of air holes due to high temperature. Afterwards, the cores of TSHF and SMF were manually aligned with the aid of a light source and a power meter. In manual splicing mode, arc duration time and arc power were set to 140 ms and 100 units. The spliced point was sufficiently robust to conduct the measurements after 7 times of arc discharges. The splice loss with SMF and the attenuation of the fiber measured by cut-back method were 0.5 dB/splice and ~0.5 dB/m at 1550 nm, respectively. The transmission spectrum was obtained using a supercontinuum source (YSL Photonics SC-5) and an optical spectrum analyzer (OSA, Yokogawa AQ6375) with a resolution of 0.02 nm. To make the sensor simple and compatible with practical applications, a polarization controller (PC) was not incorporated in the experiment. With the optimized length of TSHF, the absence of a PC does not limit the quality of transmission, where a polarization extinction ratio of above 20 dB is obtained in the interference fringes. The TSHF was mounted to the center of the fiber rotators. The fiber was kept straight to eliminate any possible bending effects, by applying a small axial tension to the fiber. The twist was performed by rotating one of the two stages from 0° to 400° with an increment of 10° in the clockwise direction while the other stage was kept fixed. Twist sensitivities were measured at room temperature (~24°C) and then to observe the environmental perturbations, temperature and strain coefficients were recorded while twisting the fiber. The measurements were carried out separately under the same experimental conditions to calibrate directional torsion, temperature and strain.

In principle, light launched into a 3-dB coupler is divided into two beams that travel through the same pathway (i.e., TSHF) in opposite directions. The phase birefringence (B) of the fiber is the difference between the effective refractive indices at the slow and fast axes (n_s−n_f). The phase difference (φ) is a function of phase birefringence (φ=$2\pi BL/\lambda$), where λ is the operating wavelength and L is the fiber length. Assuming the applied force acts in the transverse plane and does not vary in the axial direction, the fiber subjected to a torsion, which is the act of a twist, is deformed and an isotropic stress distribution is formed. Twisting of the fiber induces photoelastic effect and consequently causes variation in the birefringence as expressed in Eq. (1).

$$\Delta B = \Delta n_s - \Delta n_s = (g_s n_s - g_f n_f)\tau, \tag{1}$$

where, Δn_s, Δn_f are the variation of the effective refractive indices at the slow and fast axes and g_s, g_f are the photoelastic coefficients at the slow and fast axes, respectively. τ is the twist rate which is defined as θ/L, where θ represents the applied twist angle. The optical transmission of a Sagnac loop can be described as [19]

$$T = \frac{1 - \cos(\varphi)}{2}. \tag{2}$$

According to the change of phase difference and the fringe spacing, the wavelength shift of resonance dip in the transmission spectrum can then be defined as [19]

$$d\lambda = \frac{\Delta\lambda\Delta\varphi}{2\pi}, \tag{3}$$

where, $\Delta\lambda$ is the fringe spacing between two adjacent dips ($\Delta\lambda$=λ^2/GL). The group birefringence (G) can be calculated based on phase birefringence as $G = B - \lambda\frac{dB}{d\lambda}$. Assuming the fiber length remains constant during applied torsion [13,15,17,20], the change of phase difference can be described as $\Delta\varphi = \frac{2\pi L}{\lambda}\Delta B$. Consequently, by substituting the value of $\Delta\lambda$ and $\Delta\varphi$ in Eq. (3), the wavelength shift of the resonance dip as a function of twist rate can be defined as [17,20]

$$d\lambda = \frac{(g_s n_s - g_f n_f)\lambda\tau}{G}. \tag{4}$$

The twist-induced shear stress introduces a component of linear and circular birefringence. In a low-birefringent fiber, since the presence of linear birefringence is smaller than circular

Optics EXPRESS

birefringence, the wavelength shift occurs due to the extra circular birefringence [14]. In most of the highly-birefringent fibers, the linear birefringence is dominant and the variation ($dT/d\tau$) can be considered to be a constant, which is however, strongly dependent on the fiber structure [13], and the twist-induced wavelength shift can be expressed as a linear function of the twist angle over a specific rotational range [11,21]. Hence, the sensitivity of a twist sensor based on a high-birefringent fiber is not as large as that based on a low-birefringent fiber.

3. Twist sensing

The transmission spectra of the proposed sensor with twist angles varying from 0° to 90° in the clockwise direction are shown in Fig. 2(a). The noise present in the spectral region around 1380 nm is from the supercontinuum source. There are three prominent resonant dips located at 1417.2, 1315.3 and 1230.7 nm (dip A, B and C, respectively, in the wavelength range from 1200-1450 nm) in the transmission spectrum prior to the application of any twist. The free spectral range (FSR), which refers to the wavelength separation between two adjacent dips ($\Delta\lambda$), are 101.9 nm between dip A and dip B, and 84.6 nm between dip B and dip C, providing a wide detection span. Non-uniform spacing of FSR in the spectrum is caused by the chromatic dispersion characteristic of the group birefringence that is higher at longer wavelength [16,18]. The FSR increases with an increase in twist and the resonance dips in the interference pattern result in different twist-induced wavelength shifts. For instance, dip A moves faster towards a longer wavelength in the interference pattern compared to the speeds of dip B and C. Linear fitting over the range from 0° to 40°, resulted in twist sensitivities of 0.98, 0.39 and 0.16 nm/° for dip A, B and C, respectively.

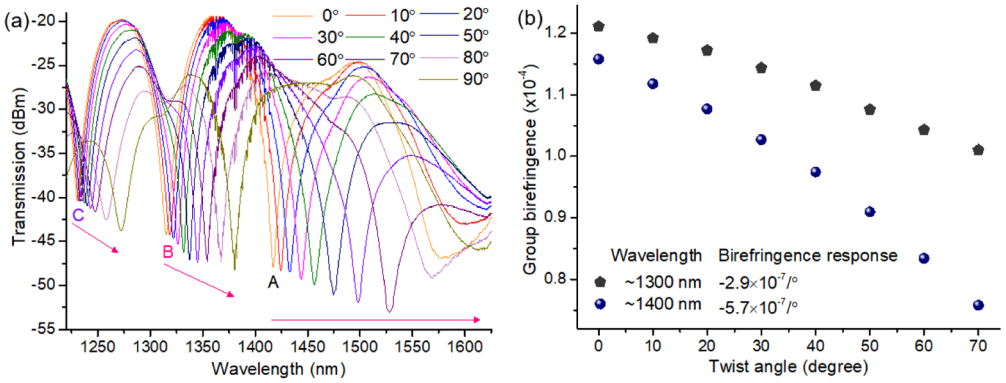

Fig. 2. (a) Measured transmission spectra at twist angles from 0°-90° and (b) the dependence of group birefringence on the twist angle of the fiber.

The variation of the group birefringence of TSHF with respect to the twist angle is presented in Fig. 2(b). Twisting the fiber from 0°-70° decreases the measured group birefringence from 1.21×10^{-4} to 1.01×10^{-4} and 1.16×10^{-4} to 0.75×10^{-4}, and twist-induced birefringence changes of -2.9×10^{-7}/° and -5.7×10^{-7}/° were observed around 1300 nm and 1400 nm, respectively. The group birefringence, which is inversely proportional to the FSR as $G=\lambda^2/\Delta\lambda L$, reduces with increasing twist angle. In previous research studies [16,18], a decrease in the FSR in the interference spectrum and a small increase in the group birefringence have been observed as a result of twisting. In contrast to these reported fiber structures, the slow axis of the elliptical core of the proposed TSHF is orthogonal to the air-holes, thus, the opposite takes place. Moreover, the core deformation of the TSHF is large due to its asymmetrical air-hole structure and the high ratio of air to silica in the cross-section of the fiber. Therefore, this configuration is more effective and can be considered more suitable for twist sensing.

Optics EXPRESS

In an effort to characterize the sensor at a high degree of twist angle, the changes in the interference fringes when twisting the fiber from 110° to 190° and 230° to 300° are shown in Figs. 3(a) and 3(b), respectively. When twisting the sensor beyond 100°, dip A exceeds 1650 nm which is outside the measured window. The three resonance dips B, C and D appear at the wavelengths of 1407.1, 1301.2 and 1229.6 nm, respectively, at the twist angle of 110° as shown in Fig. 3(a). Since the wavelength shifts of the dips behave non-monotonously, dip B shifts faster with applied twist whereas, dip C and D shift slowly at different rates. Similarly, in Fig. 3(b), when twisting is applied from 230° to 300°, dip C shifts at a faster speed but, dip D and E shift slowly at different rates. The sensitivity of the sensor was recorded up to 400° and the transmission spectra of dips D and E when twisting the fiber from 310° to 390° are plotted in Fig. 3(c). Noticeably, a large wavelength shift occurs in dip D when twisting the sensor over 370°.

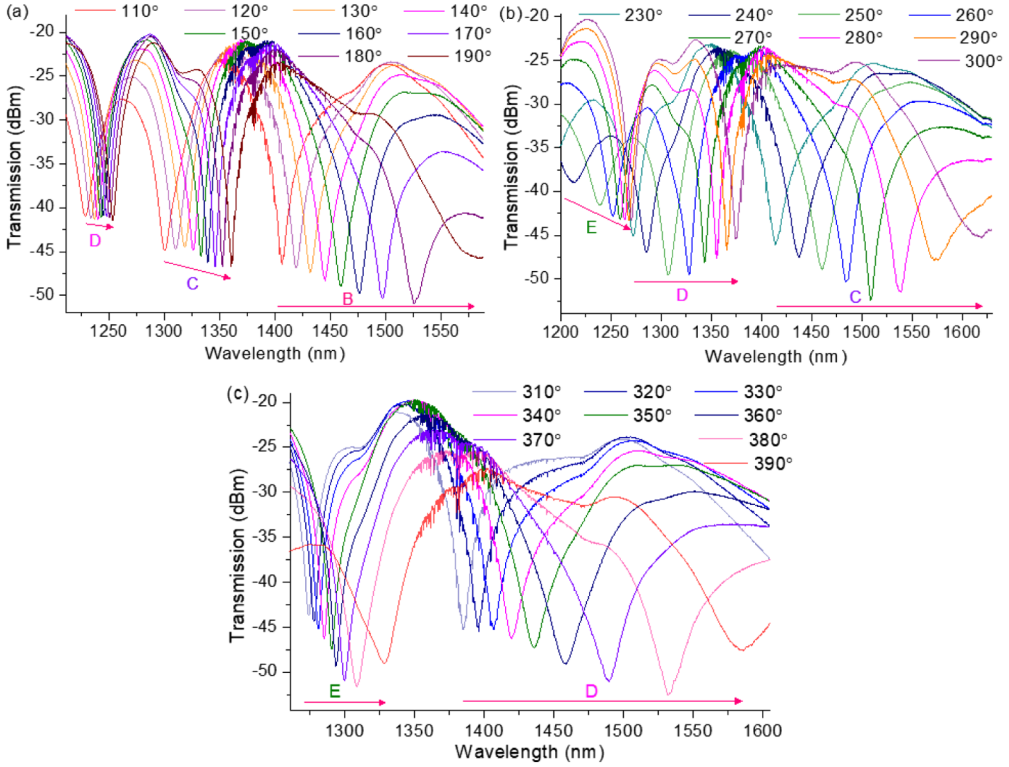

Fig. 3. Response of (a) dip B, C and D at twist angles from 110°-190°, (b) dip C, D and E at twist angles from 230°-300° and (c) dip D and E at twist angles from 310°-390° in the clockwise direction.

The contrasts of the interference fringes are above 20 dB under any twist applied to the fiber. When the fiber is subjected to a twist, the change in the polarization state of the incident light results in a variation of the intensity of each resonance dip. Parts of the intensity response exhibit a sinuous relationship which maybe mainly caused by the twist-induced circular birefringence. The loss variation with twist angle of our proposed sensor is smaller than those that were previously reported [22,23], where the twist angle ranged only up to 10° with the highest sensitivity of 0.717 dB/° in a silver-coated hollow core fiber. Owing to the limitation of the twist angle range in an intensity-based measurement, the relationship between the wavelength shift and the twist angle is preferable and provides reliable information.

Optics EXPRESS

Figure 4 summarizes the measured wavelength shift as a function of mechanical torsion when twisting the sensor from 0° to 400° in a clockwise direction. To evaluate the repeatability of the sensor during twist measurements, the experiment was repeated three times and error bars for each data point are shown in the figure. The patterns of the curves are not identical, but the dips shift rapidly at the wavelength beyond 1500 nm. The wavelength shifts of the sensor adopt a nonlinear response for a certain twist range. The responses of dip A and B, and parts of curves in dip C and D were found to have very good quadratic relationship with the torsion angle. The black lines represent the quadratic fits in a particular twist range and the fitting parameters are presented in Table 1. The accuracies in terms of percentages of the indicated R^2 values vary between 99.1% and 99.9% depending on the applied twist angle and the individual dip in the transmission spectrum. According to the linear fits associated with different ranges of twist angles, the sensitivities were more than 3.6 nm/° in dip A and B for twist angles over 50° and 150°, respectively. The sensitivities were less than 1 nm/° in dip C and D for twist angles of up to 200°, but sensitivities as high as 3.6 and 5 nm/° were observed, over twist angle ranges from 270°-300° and 370°-400°, respectively. However, it is important to note that a high twist sensitivity of 5 nm/° can be achieved at any twist angle by pre-twisting the sensor. For example, a sensitivity of 5 nm/° can be obtained over the entire twist angle range of 0°-40° by pre-twisting the sensor by 370°.

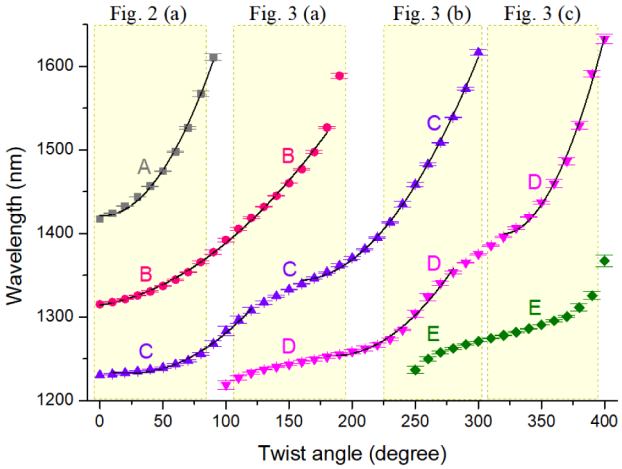

Fig. 4. The relationship between the wavelength shift of the resonance dips and the applied twist angle.

Table 1. Coefficients of the quadratic function ($y = b_0 + b_1 x + b_2 \times^2$) used to fit the curves in Fig. 4.

Dip	Twist angle	b_0	b_1	b_2	R^2 (%)
A	0°-90°	1421.87	-0.14	2.44×10^{-2}	99.61
B	0°-180°	1314.29	0.24	5.02×10^{-3}	99.81
C	10°-120°	1237.32	-0.39	8.27×10^{-3}	99.22
	150°-300°	1657.42	-4.02	1.29×10^{-2}	99.90
D	180°-280°	1647.25	-4.26	1.15×10^{-2}	99.07
	320°-400°	5019.78	-22.72	3.57×10^{-2}	99.48

Optics EXPRESS

4. Discrimination of torsion, strain and temperature

The TSHF exhibits a large change of twist-induced group birefringence due to the orientation of the fiber core and large, unsymmetrical air-hole structure. The change in the group birefringence not only results in wavelength responses with different rates for multiple resonance dips in the interference spectrum, but is also well suited for eliminating temperature and strain cross-sensitivity and for discriminating torsion, temperature and/or strain, simultaneously [8,15,16,20,24]. Depending on the applied twist, strain and temperature changes, the corresponding wavelength shifts of the multiple dips can be presented at the same time using the following algebraic expression,

$$\begin{pmatrix} \Delta\lambda_1 \\ \Delta\lambda_2 \\ \Delta\lambda_3 \end{pmatrix} = \begin{pmatrix} \psi_{\theta 1} & \psi_{S1} & \psi_{T1} \\ \psi_{\theta 2} & \psi_{S2} & \psi_{T2} \\ \psi_{\theta 3} & \psi_{S3} & \psi_{T3} \end{pmatrix} \begin{pmatrix} \Delta\theta \\ \Delta S \\ \Delta T \end{pmatrix}. \tag{5}$$

The coefficients of the matrix (ψ) are obtained experimentally by measuring the wavelength shifts of three resonance dips induced through external perturbations.

The sensitivities of resonance dips in an interference spectrum of TSHF are significantly different based on the effect of the physical parameters. According to the resonance wavelength shift of dips C, D and E, the corresponding twist sensitivities were measured to be 3.58, 1.15 and 0.41 nm/°, respectively, with an R^2 value of above 99%, based on linear fitting from 270° to 300° and the results are shown in Fig. 5. The response of dip C exhibits a difference of over 3-8 times in twist sensing when compared with the other two. Initially, the curve of dip D moves gradually, followed by an abrupt increase leading to a maximum wavelength separation of beyond 292 nm, resulting in the highest twist sensitivity of 5.01 nm/° with an R^2 of 99.1% over the twist angles ranging from 370°-400°. Therefore, the sensor is applicable in discriminating the torsion direction by tracing the different responses occurred between the clockwise and counterclockwise rotations when pre-twisting the fiber around 360°. With this highest sensitivity, a torsion resolution of 0.004° can be obtained with consideration of the OSA's resolution of 0.02 nm. Furthermore, an accurate value for the twist angle can be acquired since the sensor is capable of discriminating both strain and temperature effects.

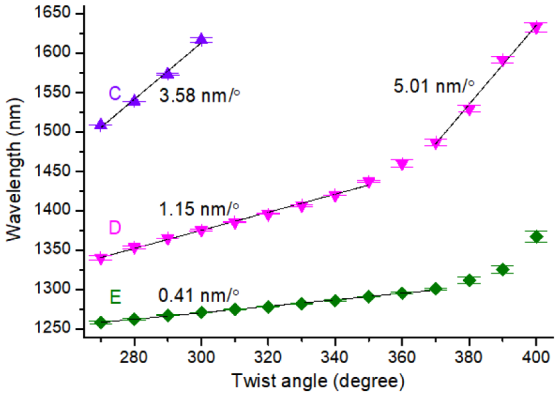

Fig. 5. The wavelength responses of dip C, D and E with respect to applied twist angles from 270°-400°. Straight lines represent the linear fits of the measured data.

The strain and temperature responses of the sensor were characterized by pre-twisting the TSHF at 270° to enhance the practicality of the sensor. To measure the axial strain, the sensing fiber was pre-twisted and stretched by moving a translation stage along z-axis and the ratio of the elongation of the stretched fiber to its original length was obtained. The strain responses

Optics EXPRESS

of the sensor measured after pre-twisting the fiber at 270° are shown in Fig. 6(a) where the inset shows the response of dip D as a function of applied strain. The dips C, D and E shift about 1.7, 2.8 and 2.6 nm to a shorter wavelength when the strain varies from 0 to 2027 με with an increment of 203 με. Due to the wavelength dependence of the strain sensitivity, there is a small discrepancy in the curves [25]. However, the experiment was repeatable, and the strain coefficients of dips C, D and E are obtained as −0.86, −1.32 and −1.24 pm/με, respectively. In order to investigate the temperature response of the sensor, the sensing fiber was heated from 40 °C to 160 °C under a pre-twisting condition. Fig. 6(b) demonstrates the temperature responses of the dips in the interference spectrum and the curves blue shift with increasing temperature. Due to the chromatic dispersion characteristics in the interference fringes, different wavelength responses occur at individual dips [18] whereas, the shorter the wavelength of the dip, the higher the temperature sensitivity. The wavelength blue shifts up to 18.3 nm in dip E operating between 1253.7 and 1235.4 nm when the temperature increased from 40 °C to 160 °C as shown in the inset in Fig. 6(b). The thermal coefficients of dips C, D and E are −0.10, −0.13 and −0.16 nm/°C, respectively. The strain responses of dips D and E have nearly the same gradient values, but dip E shows a higher temperature response. A small change is observed in the sensitivity of dip C which has a lower strain and temperature response. Particularly for strain response, the inconsistency occurred in dip C might be the existence of second-order mode in the fiber when operating at long wavelength [25,26]. Since the strain and temperature coefficients of the sensor are significantly different, the proposed sensor is well suited to discriminate the three parameters.

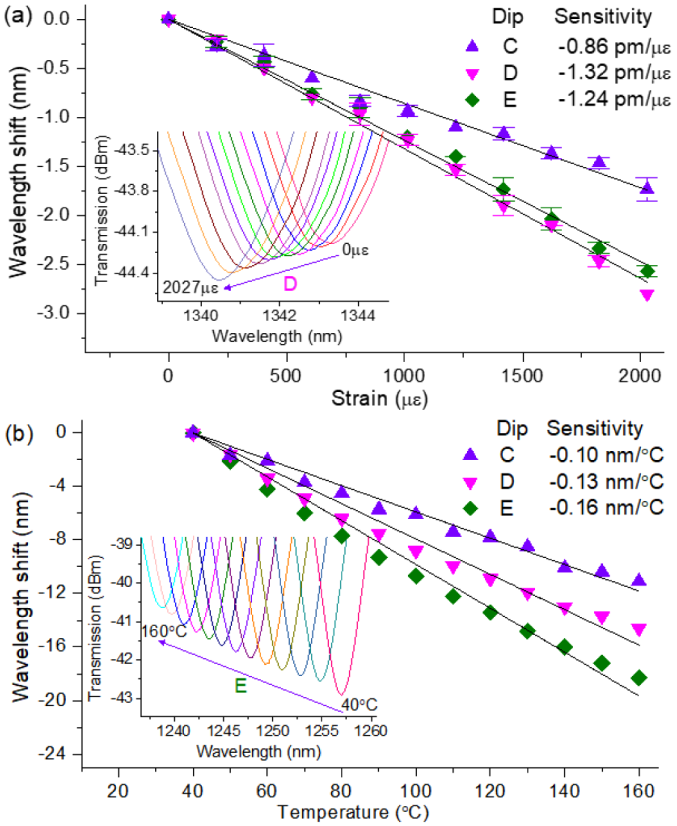

Fig. 6. (a) The strain-induced wavelength shift and (b) temperature response of the sensor at a twist angle of 270°. Straight lines are the linear fits of the measured data.

Optics EXPRESS

The coefficients of the matrix for the proposed sensor were 3.58, 1.15 and 0.41 nm/° for torsion, −0.86, −1.32 and −1.24 pm/με for strain, and −0.10, −0.13 and −0.16 nm/°C for temperature when the wavelengths of the three dips were around 1508.9, 1343.2 and 1259.2 nm. The matrix (ψ) in Eq. (5) can be rewritten with the coefficients obtained experimentally as,

$$\psi = \begin{pmatrix} 3.58 & -0.86\times10^{-3} & -0.10 \\ 1.15 & -1.32\times10^{-3} & -0.13 \\ 0.41 & -1.24\times10^{-3} & -0.16 \end{pmatrix}. \tag{6}$$

The matrix (ψ) gives a nonzero determinant which was calculated to be 1.5508×10^{-4}. Hence, the matrix is well-conditioned and inverse matrix exists where the inverse of a matrix is the division of its adjunct matrix given in Eq. (7) by the determinant.

$$Adj(\psi) = \begin{pmatrix} 5.0\times10^{-5} & -1.36\times10^{-5} & -2.02\times10^{-5} \\ 0.1307 & -0.5318 & 0.3504 \\ -0.8848\times10^{-3} & 4.0866\times10^{-3} & -3.7366\times10^{-3} \end{pmatrix}. \tag{7}$$

Consequently, the torsion, strain and temperature variations can be independently determined by substituting the coefficients of multi-parameters to an inverted matrix form in Eq. (5) resulting in Eq. (8) as follows,

$$\begin{pmatrix} \Delta\theta \\ \Delta S \\ \Delta T \end{pmatrix} = \begin{pmatrix} 0.3224 & -0.0877 & -0.1303 \\ 842.80 & -3429.24 & 2259.51 \\ -5.7055 & 26.3519 & -24.095 \end{pmatrix} \begin{pmatrix} \Delta\lambda_1 \\ \Delta\lambda_2 \\ \Delta\lambda_3 \end{pmatrix}. \tag{8}$$

By detecting the wavelength shifts of the three dips, $\Delta\lambda_i$ (i=1, 2, 3), measured in nanometer, simultaneous changes of the corresponding parameters ($\Delta\theta$, ΔS and ΔT) can be calculated where their units are in angular degree, microstrain and degree Celsius, respectively. The resolutions of the parameters can be estimated by the absolute value of the inverse matrix multiplied by the wavelength measurement errors, $\delta(\Delta\lambda_i)$ (i =*1,2,3*), as follows,

$$\begin{pmatrix} \delta(\Delta\theta) \\ \delta(\Delta S) \\ \delta(\Delta T) \end{pmatrix} = |\psi^{-1}| \begin{pmatrix} \delta(\Delta\lambda_1) \\ \delta(\Delta\lambda_2) \\ \delta(\Delta\lambda_3) \end{pmatrix}. \tag{9}$$

Considering a detection system with the wavelength resolution of 0.02 nm, the resolutions of torsion, strain and temperature of the proposed sensor can be estimated as ±0.01°, ±130.6 με and ±1.1°C, respectively over the measurement ranges of 270°-300°, 0-2027 με and 40-160 °C. It should be noted that, in spite of its poor strain resolution, the proposed sensor offers better torsion and temperature resolutions when compared to the others [15,16,27].

The proposed sensing configuration can also discriminate other pairs of physical parameters, e.g., torsion-strain or torsion-temperature by monitoring only two dips in the transmission spectrum by solving the following matrix equations.

$$\begin{pmatrix} \Delta\lambda_1 \\ \Delta\lambda_2 \end{pmatrix} = \begin{pmatrix} \psi_{\theta1} & \psi_{S1} \\ \psi_{\theta2} & \psi_{S2} \end{pmatrix} \begin{pmatrix} \Delta\theta \\ \Delta S \end{pmatrix}, \tag{10}$$

Optics EXPRESS

$$\begin{pmatrix} \Delta\lambda_1 \\ \Delta\lambda_2 \end{pmatrix} = \begin{pmatrix} \psi_{\theta 1} & \psi_{T1} \\ \psi_{\theta 2} & \psi_{T2} \end{pmatrix} \begin{pmatrix} \Delta\theta \\ \Delta T \end{pmatrix}, \tag{11}$$

where, $\Delta\lambda_1$, $\Delta\lambda_2$ are the wavelength shifts of two dips in the transmission spectrum. The discrimination of the corresponding pair of parameters ($\Delta\theta$ and ΔS, or $\Delta\theta$ and ΔT) can be determined by substituting the coefficient of matrix (ψ) obtained from the slope/gradient of the experimental data. The discriminations of torsion and strain measurements were performed using dip C and D operating at 1508.9 nm and 1343.2 nm and dip C and E operating at 1508.9 nm and 1259.2 nm, respectively. The coefficient of matrix, determinant of matrix (ψ), inverted matrix and resolution of the sensing parameters are shown in Table 2. Particularly, as a result of large difference in coefficients of torsion sensing, the pair of dip C and E provides a better torsion and strain discrimination with resolutions of ±0.01° and ±19.5 με, respectively. As in the case of torsion and strain, the discrimination of torsion and temperature can be deduced by substituting the coefficients of dip C and D pair, and dip C and E pair in Eq. (11). The wavelengths of dip C, D and E were located at 1508.9 nm, 1343.2 nm, and 1259.2 nm, respectively. Together with the coefficients of matrix obtained experimentally, determinant of matrix (ψ), inverted matrix and resolution are given in Table 3. Similarly, the latter pair, i.e. dip C and E, indicates better resolutions which were estimated to be ±0.01° and ±0.15°C for torsion and temperature measurements, respectively. As expected, the responses of dip C and E operating at wavelengths of around 1508.9 nm and 1259.2 nm provide better results but a broader detection range will be required in the measurement system. Evidently, detecting more parameters at the same time decreases the accuracy of the sensor. The discriminations of torsion-strain pair and torsion-temperature pair enhance the resolutions of strain and temperature when compared with discrimination of all three parameters.

Table 2. Coefficients of matrix and parameters for discrimination of torsion and strains.

Dip	Matrix ψ	Determinant	Inverse of ψ	Resolution
C, D	$\begin{bmatrix} 3.58 & -0.86\times10^{-3} \\ 1.15 & -1.32\times10^{-3} \end{bmatrix}$	-3.7366×10^{-3}	$\begin{bmatrix} 0.3533 & -0.2302 \\ 307.766 & -958.09 \end{bmatrix}$	±0.012°±25.3 με
C, E	$\begin{bmatrix} 3.58 & -0.86\times10^{-3} \\ 0.41 & -1.24\times10^{-3} \end{bmatrix}$	-4.0866×10^{-3}	$\begin{bmatrix} 0.3034 & -0.2104 \\ 100.328 & -876.034 \end{bmatrix}$	±0.010°±19.5 με

Table 3. Coefficients of matrix and parameters for discrimination of torsion and temperature.

Dip	Matrix ψ	Determinant	Inverse of ψ	Resolution
C, D	$\begin{bmatrix} 3.58 & -0.10 \\ 1.15 & -0.13 \end{bmatrix}$	−0.3504	$\begin{bmatrix} 0.3710 & -0.2854 \\ 3.2820 & -10.2169 \end{bmatrix}$	±0.013°±0.27°C
C, E	$\begin{bmatrix} 3.58 & -0.10 \\ 0.41 & -0.16 \end{bmatrix}$	−0.5318	$\begin{bmatrix} 0.3009 & -0.1880 \\ 0.7710 & -6.7319 \end{bmatrix}$	±0.010°±0.15°C

5. Discussion

In order to evaluate the performance of the proposed sensor, a comparison between our experimental results and other related research studies is provided in Table 4 where the sensitivities together with the ranges of twist angles are summarized. The reported sensors have been constructed based on SI using different types of optical fibers. The sensitivity of the proposed sensor is about fifty nine times higher than the sensors in side-hole fibers [16,17] and over five times higher than the sensors in PM-elliptical core fiber [20] and PCFs [14,15]. By opting out

Optics EXPRESS

the usage of any special fiber in SI, a straight-line waveguide channel has been inscribed in the cladding of an SMF by a femtosecond laser to introduce an unsymmetrical stress distribution in which a sensitivity of up to 3.26 nm/° in the range of −10°-80° with R^2 of 97.2% and that of 2.37 nm/° in 180°-270° with R^2 of 99.8% have been observed [8]. The sensor itself has low temperature and strain cross-sensitivities but the transmission spectra of the sensor lack clarity. The twist range of proposed sensor is narrower than that of the other sensors listed in Table 4. Although the sensitivities of the sensors based on the side-hole fibers are small, they can provide a wide range of twist angles of up to 350° or 291° in both clockwise and counterclockwise directions. The sensor based on the PM-elliptical core fiber offers a measurement range of up to 120° whereas the highly sensitive twist sensors listed in the 4^{th}-7^{th} row of the table are incapable of reaching twist angles beyond a range of 90°. This may possibly be due to the limitation of the wavelength range of the source or the detector in observing a large change in the spectrum. On the contrary, fringe visibility and FSR of the spectrum may not be considerably large to be detected. The sensor length can greatly contribute to optimize the sensitivity, resolution and fringe spacing. According to the 16-cm long sensor used in our experiment, the rate of change of twist per unit length of the sensor can be estimated as 0.8 nm/° m^{-1} which corresponds to the maximum twist sensitivity. It is larger than the sensors based on the side-hole fibers and the side-leakage PCF in which 0.038-0.076 nm/° m^{-1} and 0.14 nm/° m^{-1} have been recorded for sensing lengths of 45-95 cm and 14.85 cm, respectively.

Table 4. Comparison of the current study with previously reported SI-based twist sensors.

	Fiber	Highest twist Sensitivity (nm/°)	Twist range (degree)	Temperature (nm/°C)	Strain (pm/με)	Ref.
1	PM side-hole fiber	0.08	0 to 360	−1.97 to −1.44	−16 to −21	[16]
2	Side-hole fiber	0.085	±291	-	4.3	[17]
3	PM-elliptical core fiber	0.68	0 to 120	−0.29 to −0.43	-	[20]
4	Side-leakage PCF	0.94	0 to 80	0.051 to 0.068	-	[15]
5	Low birefringence PCF	1.00	60 to 140	−0.5	-	[14]
6	Femtosecond laser-inscribed waveguide in SMF	3.26	−10 to 80	−0.00018	0.045	[8]
7	Two semicircular-hole fiber	5.01	370 to 400	−0.09 to −0.15	−0.8 to −1.37	current study

Although the response of the sensor is not linear in the entire sensing range of 0°-400°, the highest twist sensitivity is obtained by linearly fitting over the range from 370°-400°. The twist sensitivity of 5.01 nm/° for twist angles varying from 370° to 400°, obtained in this work, is the highest value reported in SI-based twist sensors, to the best of our knowledge. However, the twist measurement range depends on the twist angle range of interest when performing the linear fit, since the dips shift rapidly at wavelengths beyond 1500 nm. For instance, based on the linear fitting from 220°-290° and 270°-300°, the response of dip C exhibits twist sensitivities of 2.52 and 3.58 nm/° (see Fig. 4) with R^2 values of above 99% in the wavelength regimes of 1395-1573 nm and 1509-1617 nm, respectively. For the twist angle range from 220°-290°, a broader measurement range with a lower twist sensitivity is observed when compared to the linear fit from 270°-300°. In addition, a high sensitivity with a broad measurement range can be observed when the measurements are conducted under a lower R^2 value which results in a larger

Optics EXPRESS

variation in the measured data and fitted values. A sensitivity of 2.83 nm/° was obtained for Dip C by linearly fitting over the range from 230°-300° with an R^2 value of 98.4%.

Apart from having a large twist sensitivity, the proposed sensor also possesses the capability to determine strain and temperature perturbations and distinguish the direction of torsion. By exploiting the wavelength shifts of three resonance dips in an interference pattern, we propose a scheme to discriminate torsion, strain and temperature variations. The sensors in the PM side-hole fiber [16], the PM-elliptical core fiber [20] and the low birefringence PCF [14] also involve twist, temperature and/or strain discrimination mechanisms. Among them, temperature and strain sensitivities in the PM side-hole fiber [16] provide highest responses compared with SI-based twist sensors in Table 4. The proposed sensor has a low sensitivity towards axial strain because of the isolation of the fiber core, and its temperature sensitivity is high due to the low birefringence of the fiber and the incorporation of Ge in the fiber core. However, the temperature sensitivity is lower than that of the side-hole fibers [16,17] and the low birefringence PCF. According to its highest twist sensitivity and capability to discriminate axial strain and temperature, the proposed sensor is preferable for applications where precision measurement is required especially for small twist angle regimes.

6. Conclusion

We have presented a highly sensitive twist sensor by inserting a segment of a novel two semicircular-hole fiber which contains an elliptical core, a rectangular strut and two semicircular-holes into a Sagnac loop. The two semicircular-hole fiber with an unsymmetrical air-hole structure introduces a high deformation in the fiber core through mechanical torsion and a large change of group birefringence in the interference fringes. The highest twist sensitivity of 5.01 nm/° was obtained for twist angles ranging from 370°-400°. It is over five orders in magnitude higher than similar reported sensors using various microstructured optical fibers in a Sagnac loop. The sensor is also applicable in the discrimination of the torsion direction as it provides a sensitivity of 1.15 nm/° over a twist angle range from 270°-350°. Moreover, the sensor reacts with different wavelength responses to the physical parameters at different resonance dips. By monitoring the wavelength shift of three resonance dips in the interference pattern, the sensor can detect directional torsion and is also capable of discriminating strain and temperature perturbations. In the angle measurement between 270°-300°, the twist sensitivities of three resonance dips were 3.58, 1.15 and 0.41 nm/° where the strain and temperature sensitivities were found to be −0.86, −1.32, and −1.24 pm/με, and −0.10, −0.13, and −0.16 nm/°C, respectively. Therefore, the proposed twist sensor is highly desirable for practical applications due to its various advantages such as ease of fabrication, high sensitivity, and discrimination of torsion, temperature and strain as well as rotational direction discrimination.

Funding

The Hong Kong Polytechnic University (1-ZVGB); CNERC (Project BBVH); National Natural Science Foundation of China (61827820, 61905096).

Disclosures

The authors declare no conflicts of interest related to this article.

References

1. R. Xu, A. Yurkewich, and R. V. Patel, "Curvature, torsion, and force sensing in continuum robots using helically wrapped FBG sensors," IEEE Robot. Autom. Lett. **1**(2), 1052–1059 (2016).
2. C. Rodrigues, C. Félix, A. Lage, and J. Figueiras, "Development of a long-term monitoring system based on FBG sensors applied to concrete bridges," Eng. Struct. **32**(8), 1993–2002 (2010).

Optics EXPRESS

3. W. Yiping, M. Wang, and X. Huang, "In fiber Bragg grating twist sensor based on analysis of polarization dependent loss," Opt. Express **21**(10), 11913–11920 (2013).
4. B. Huang and X. Shu, "Ultra-compact strain- and temperature-insensitive torsion sensor based on a line-by-line inscribed phase-shifted FBG," Opt. Express **24**(16), 17670–17679 (2016).
5. W. Liu, C. Sun, Y. Ma, X. Bai, L. Yu, S. Duan, H. Du, C. Zhao, C. Lu, and L. Zhao, "A highly sensitive torsion sensor with a new fabrication method," IEEE Photonics Technol. Lett. **31**(6), 463–466 (2019).
6. H. Zhang, Z. Wu, P. P. Shum, X. Shao, R. Wang, X. Q. Dinh, S. Fu, W. Tong, and M. Tang, "Directional torsion and temperature discrimination based on a multicore fiber with a helical structure," Opt. Express **26**(1), 544–551 (2018).
7. Z. Bai, M. Deng, S. Liu, Z. Zhang, J. Xu, J. Tang, Y. Wang, C. Liao, and Y. Wang, "Torsion sensor with rotation direction discrimination based on a pre-twisted in-fiber Mach–Zehnder interferometer," IEEE Photonics J. **9**(3), 1–8 (2017).
8. B. Huang and X. Shu, "Highly sensitive torsion sensor with femtosecond laser-induced low birefringence single-mode fiber based Sagnac interferometer," Opt. Express **26**(4), 4563–4571 (2018).
9. B. Huang and X. Shu, "Highly sensitive twist sensor based on temperature- and strain-independent fiber Lyot filter," J. Lightwave Technol. **35**(10), 2026–2031 (2017).
10. V. Budinski and D. Donlagic, "Fiber-optic sensors for measurements of torsion, twist and rotation: a review," Sensors **17**(3), 443 (2017).
11. Z. Liu, C. Wu, M.-L. V. Tse, and H.-Y. Tam, "Fabrication, characterization, and sensing applications of a high-birefringence suspended-core fiber," J. Lightwave Technol. **32**(11), 2113–2122 (2014).
12. O. Frazão, R. M. Silva, J. Kobelke, and K. Schuster, "Temperature- and strain-independent torsion sensor using a fiber loop mirror based on suspended twin-core fiber," Opt. Lett. **35**(16), 2777–2779 (2010).
13. H.-M. Kim, T.-H. Kim, B. K. Kim, and Y. Chung, "Temperature-insensitive torsion sensor with enhanced sensitivity by use of a highly birefringent photonic crystal fiber," IEEE Photonics Technol. Lett. **22**(20), 1539–1541 (2010).
14. P. Zu, C. C. Chan, Y. Jin, T. Gong, Y. Zhang, L. H. Chen, and X. Dong, "A temperature-insensitive twist sensor by using low-birefringence photonic-crystal-fiber-based Sagnac interferometer," IEEE Photonics Technol. Lett. **23**(13), 920–922 (2011).
15. W. Chen, S. Lou, L. Wang, H. Zou, W. Lu, and S. Jian, "Highly sensitive torsion sensor based on Sagnac interferometer using side-leakage photonic crystal fiber," IEEE Photonics Technol. Lett. **23**(21), 1639–1641 (2011).
16. O. Frazão, S. O. Silva, J. M. Baptista, J. L. Santos, G. Statkiewicz-Barabach, W. Urbanczyk, and J. Wojcik, "Simultaneous measurement of multiparameters using a Sagnac interferometer with polarization maintaining side-hole fiber," Appl. Opt. **47**(27), 4841–4848 (2008).
17. T. Liu, H. Zhang, L. Xue, B. Liu, H. Liu, B. Huang, J. Sun, and D. Wang, "Highly sensitive torsion sensor based on sidehole-fiber Sagnac interferometer," Sensors **19**(17), 7378–7382 (2019).
18. X. Wang, S. Lou, X. Sheng, and S. Liang, "Simultaneous measurement of torsion, strain and temperature using a side-leakage photonic crystal fiber loop mirror," Infrared Phys. Technol. **76**, 603–607 (2016).
19. X. Dong, H.-Y. Tam, and P. Shum, "Temperature-insensitive strain sensor with polarization-maintaining photonic crystal fiber based Sagnac interferometer," Appl. Phys. Lett. **90**(15), 151113 (2007).
20. B. Song, H. Zhang, Y. Miao, W. Lin, J. Wu, H. Liu, D. Yan, and B. Liu, "Highly sensitive twist sensor employing Sagnac interferometer based on PM-elliptical core fibers," Opt. Express **23**(12), 15372–15379 (2015).
21. A. J. Barlow, J. J. Ramskov-Hansen, and D. N. Payne, "Birefringence and polarization mode-dispersion in spun single-mode fibers," Appl. Opt. **20**(17), 2962–2968 (1981).
22. Y. Chen, Y. Semenova, G. Farrell, F. Xu, and Y.-Q. Lu, "A compact Sagnac loop based on a microfiber coupler for twist sensing," IEEE Photonics Technol. Lett. **27**(24), 2579–2582 (2015).
23. D. Liu, R. Kumar, F. Wei, W. Han, A. K. Mallik, J. Yuan, C. Yu, Z. Kang, F. Li, Z. Liu, H.-Y. Tam, G. Farrell, Y. Semenova, and Q. Wu, "Highly sensitive twist sensor based on partially silver coated hollow core fiber structure," J. Lightwave Technol. **36**(17), 3672–3677 (2018).
24. Y. Li, P. Lu, Z. Qu, W. Zhang, W. Ni, D. Liu, and J. Zhang, "An optical fiber twist sensor with temperature compensation mechanism based on T-SMS structure," IEEE Photonics J. **12**(1), 1–8 (2020).
25. B. K. Kim, S. H. Yun, I. K. Hwang, and B. Y. Kim, "Nonlinear strain response of two-mode fiber-optic interferometer," Opt. Lett. **21**(13), 934–936 (1996).
26. H. Zhang, Z. Wu, P. P. Shum, X. Q. Dinh, C. W. Low, Z. Xu, R. Wang, X. Shao, S. Fu, W. Tong, and M. Tang, "Highly sensitive strain sensor based on helical structure combined with Mach-Zehnder interferometer in multicore fiber," Sci. Rep. **7**(1), 46633 (2017).
27. K. Naeem, B. H. Kim, B. K. Kim, and Y. Chung, "Simultaneous multi-parameter measurement using Sagnac loop hybrid interferometer based on a highly birefringent photonic crystal fiber with two asymmetric cores," Opt. Express **23**(3), 3589–3601 (2015).